Available online at www.sciencedirect.com
ScienceDirect
Applied Catalysis B: Environmental 78 (2008) 53–60
APPLIED CATALYSIS B: ENVIRONMENTAL
www.elsevier.com/locate/apcatb

Catalytic hydrodechlorination of chlorinated ethenes by nanoscale zero-valent iron

Hocheol Song, Elizabeth R. Carraway *

Department of Environmental Engineering and Science, Clemson University, 342 Computer Court, Anderson, SC 29625, USA

Received 31 December 2006; received in revised form 26 July 2007; accepted 30 July 2007
Available online 6 August 2007

Abstract

The reduction of six chlorinated ethenes by nanoscale iron (<100 nm diameter) synthesized by borohydride reduction was studied in order to determine reaction rates and product distributions and to gain insight into reaction pathways. The transformation of chlorinated ethenes by nanoscale iron proceeded to fully dechlorinated products (ethene and ethane), with no production of chlorinated intermediates, and the reaction rate constants for disappearance of chlorinated ethenes increased with decreasing chlorination (vinyl chloride (VC) > dichloroethenes (DCEs) > trichloroethene (TCE) > tetrachloroethene (PCE)). This trend suggests the reduction of chlorinated ethenes by nanoscale iron did not occur under thermodynamic control (e.g. reduction potential), rather, it proceeded via a catalytic pathway involving reactive hydrogen species. The reduction of TCE under five different conditions of initial dissolved hydrogen concentrations which varied from about 0.02 to 1.2 mM confirmed the importance of hydrogen in the reaction pathway and revealed an excellent linear correlation between rate constant and hydrogen concentration. Reduction of a chlorinated ethane (1,1,1,2-tetrachloroethane) which produced 1,1-DCE as an intermediate, showed no dependence on hydrogen concentrations but the disappearance of the ethene intermediate did. TCE reduction by commercial grade micro-sized iron samples, in contrast, showed insignificant dependence on hydrogen concentration, suggesting the nanoscale iron synthesized by borohydride reduction of iron salts is particularly suited for hydrogen utilization through a catalytic reduction of chlorinated ethenes.

Keywords: Nanoscale iron; Boron; Hydrogen; Catalytic hydrogenation; Reductive dechlorination; Chlorinated compounds

1. Introduction

Chlorinated ethenes are some of the most commonly found groundwater pollutants. Remediation of groundwater contaminated with chlorinated ethenes has been a major environmental challenge because of their wide occurrence and limitations associated with conventional pump-and-treat approach. Permeable reactive barrier (PRB) technology utilizing zero-valent iron has been developed in an effort to find more efficient and cost effective alternatives, and it received a great deal of attention during past decade. Researchers have worked several years to extend the scope of this technology, including amended iron (e.g. palladium and nickel) [1–4] and nanoscale iron [5–9].

The use of nanoscale iron is one of the latest developments that takes advantage of unique characteristics of small-sized particles. These include very rapid destruction of contaminants [10,11], the potential for *in situ* delivery of particles to subsurface contaminants [12–16], and changes in reaction mechanism with very small particle size [17]. These characteristics make nanoscale iron a good alternative to the conventional PRB, because it can reduce potential limitations of PRB, while sustaining some of the intrinsic advantages of PRB. Nanoscale iron is suitable to apply directly to the concentrated source area or to install reactive zones under difficult conditions such as at great depth or under surface structures that prohibit trenching. This approach was successfully demonstrated in recent field applications where nanoscale iron was injected into subsurface to remediate trichloroethylene (TCE) containing groundwater and TCE dense nonaqueous phase liquid (DNAPL) [12–15].

Much research with nanoscale iron to date has focused on bimetallic nanoscale iron [9,18,19]. Bimetallic nanoscale iron is typically produced by borohydride reduction of iron salts in an aqueous phase, followed by deposition of small quantity of noble metals (e.g. 0.05–0.25 wt% Pd, Ni) on the iron surface via

* Corresponding author. Tel.: +1 864 656 5574; fax: +1 864 656 0672.
E-mail addresses: hsong@clemson.edu (H. Song), ecarraw@clemson.edu (E.R. Carraway).

0926-3373/$ – see front matter © 2007 Elsevier B.V. All rights reserved.
doi:10.1016/j.apcatb.2007.07.034

spontaneous redox reaction between a noble metal salt precursor and Fe(0). The primary effect of doping or plating iron with secondary metals is to route the reactions through more rapid catalytic pathways and increases the rate of contaminants degradation [20,4]. Such an effect has been observed for the reactions between bimetallic micro-sized iron and a number of organic contaminants including chlorinated methanes [20,21], ethenes [2,22,23], ethanes [24,25], chlorobenzenes [26,27], chlorophenols [28,29] and polychlorinated biphenyls [30]. It is notable that the lists of contaminants treatable with bimetallic iron include some classes of compounds that are impracticably slow with iron only.

The catalytic effect of noble metals stems in part from their ability to adsorb hydrogen and intercalate it within the metal lattice, forming metal hydride complexes that serve as direct reductants for adsorbed contaminants [1,31]. In bimetallic Fe(0) reactions, the primary role of iron is to produce hydrogen by reducing water and the noble metals acts as a collector of hydrogen [32]. The extent of hydrogen adsorption of noble metals depends on their hydrogen storage capability [33]. Catalytic removal of contaminants, especially for halogenated compounds, is favorable since the process produces mostly fully saturated hydrocarbon products, and thus curtails production of undesirable byproducts which often result from reactions involving unamended iron [4,32]. However, despite the promising performance of bimetallic systems, the use of bimetals has not yet been considered as a primary *in situ* remedial option due to uncertainties associated with cost, surface deactivation, and the risk of toxic effects of noble metals.

Compared to bimetallic iron, unamended iron is a much weaker catalyst since it has a much smaller hydrogen adsorption capacity [34]. However, evidence of a catalytic pathway has been reported for both micro and nanoscale iron in the reduction of TCE [6,7,35,36] and nitrosodimethylamine [37]. The catalytic pathway of TCE reduction observed for nanoscale iron was evinced by the positive correlation between hydrogen concentration and reaction rate, and the similarity in products distribution to noble metal catalyzed reaction [6,7]. The nanoscale iron produced from borohydride reduction has been reported to have core–shell structure in which inner core consists of α-Fe(0) while outer shell is composed of mainly Fe-oxides enriched with boron (less than 10 wt%) [8,10]. The presence of boron has been suggested to be responsible for the catalytic behavior of the particles [6]. Boron is a common ingredient in hydrogenation alloy catalysts (Ni–B, Co–B) for promoting catalytic activity of base metals by inducing structural and electrochemical modifications, which favor hydrogenation activity [38]. It has also been demonstrated that addition of boron enhances the extent of hydrogen absorption capacity of alloys, as well as the rate of hydrogen absorption/desorption [39]. However, Liu et al. [7] demonstrated that crystalline boron-containing iron particles did not activate hydrogen, raising the possibility that the catalytic activity observed may be due to an amorphous particle surface containing a number of structural defects.

In this study, we investigated the reactions of nanoscale iron with chlorinated ethenes to determine whether the reduction is a catalytically driven process. The ability of nanoscale iron to activate hydrogen was evaluated by investigating the role of hydrogen in the reduction process. Kinetic experiments were conducted under varying hydrogen levels to gain insight into how hydrogen affects the rate and extent of reaction. To investigate the compound specificity of catalytic reactions of nanoscale iron, the iron was also applied to chlorinated ethanes. Finally, the effect of hydrogen was examined for commercial grade micro-sized iron and compared with nanoscale iron reaction.

2. Experimental

2.1. Materials

Chemicals used in this study were tetrachloroethene (PCE) (99.9%, HPLC grade, Sigma), TCE (99.9%, HPLC grade, Sigma), *cis*-1,2-dichloroethene (*c*-DCE) (99%, HPLC grade, Sigma), *trans*-1,2-dichloroethene (*t*-DCE) (99.9%, HPLC grade, Sigma), 1,1-dichloroethene (1,1-DCE) (99.9%, HPLC grade, Sigma), vinyl chloride (VC) (5000 mg/L, Chemservice), 1,1,1,2-trichloroethane (1,1,1,2-TeCA), ethene (1000 ppm, 1% in He, Scott Specialty Gas), ethane (1000 ppm in He, Scott Specialty Gas), methanol (99.9%, HPLC grade, B&J), pentane (99.9%, GC grade, B&J), and toluene (99.9%, HPLC grade, B&J). MOPS buffer (3-(*N*-morpholino)propanesulfonic acid) was obtained from Sigma. All chemicals were used as received. Methanolic stock solutions of target compounds were prepared from pure compounds and used within 1 day. Deionized water from a Milli-Q water system (≈18 MΩ cm) was deoxygenated by purging with high purity N_2. Commercial irons were obtained from ARS Technologies, Inc. (New Jersey, NJ) (H-200), Connelly GPM Inc. (Chicago, IL) (CC-1021) and Fisher Scientific (electrolytic powder ≥99%, +100 mesh). A Micromeritics ASAP 2010 surface area analyzer using the N_2 adsorption BET method gave surface areas of 1.03(±0.01), 5.15(±0.03), and 0.18(±0.03) m^2/g for ARS, Connelly, and Fisher irons, respectively. The particles were dried under N_2 atmosphere and kept in an anaerobic chamber (5% H_2 in N_2 atmosphere, Coy) before use.

2.2. Synthesis of nanoscale iron

Nanoscale iron was synthesized by reduction of ferric chloride (98%, Aldrich, 1.2 M, 50 mL) by sodium borohydride (98%, Aldrich, 3.6 M, 50 mL), following Glavee et al. [40] except that an inert atmosphere (N_2) was maintained throughout the synthesis. Iron was washed with water three times, followed by acetone washing. Dried particles were stored in the anaerobic chamber to avoid air contact. Such precautions were taken because, if contacted with air, these particles undergo a strong exothermic oxidation reaction, usually resulting in brief flaring. The electron microscope images of the synthesized particles are consistent with the images previously reported in the literature [6–8]. The particle composition measured by a Perkin-Elmer Sciex Elan 9000 inductively coupled plasma (ICP) mass spectrometer gave iron and boron contents of 92.0 ± 0.4 and 7.0 ± 0.4 wt%,

respectively, for six samples synthesized under the same conditions. The average specific surface area, measured by a Micromeritics ASAP 2010 using BET Kr gas adsorption isotherm in the relative pressure range 0.06–0.21, was 27.9(±1.7) m^2/g for five nanoscale iron samples. This value is in good agreement with results of other studies, which range from 18 to 35 m^2/g [5–8,41].

2.3. Batch experiments

For reduction experiments, amber bottles (125 mL, VWR) sealed with Mininert® (VICI) caps and Teflon®-lined silicone septa (VWR) were used as batch reactors. Bottles containing iron (0.01–0.02 g) and water were prepared in the anaerobic chamber with minimal headspace (approximately 1 mL). Reactor and control bottles were prepared in duplicate. Reactions were initiated by injecting a known volume (typically 10–100 μL) of a methanolic stock solution of the chlorinated ethane; methanol volume fractions were less than 0.1%. All bottles were mixed end-over-end at 40 rpm and room temperature (23 ± 1 °C). Duplicate bottles were sampled periodically by withdrawing 0.5 mL of the aqueous phase with a 1 mL airtight syringe (Hamilton), followed by injection of an equal volume of water to maintain constant headspace. Aqueous samples were immediately injected into sealed 2 mL vials containing pentane (with 5 ppm toluene as an internal standard). After thorough mixing, 200 μL of the pentane extract were withdrawn and transferred to a GC autosampler vial.

2.4. Analytical methods

The analyses of chlorinated ethenes were performed using a HP G1800A GCD GC/MS equipped with a DB-VRX column (60 m, 0.25 mm, 1.8 μm, J&W Scientific). The temperature program was at 70 °C for 8 min, 20 °C/min to 160 °C, and held for 2.5 min. The sample (2 μL) was injected in split mode with a split ratio of 30:1. The carrier gas was UHP helium at 1 mL/min. The injector and detector temperatures were 230 and 300 °C, respectively. Selected ion monitoring (SIM) mode was used for data acquisition.

For ethane and ethene analyses, reactions were stopped by removal of 0.5 mL aqueous samples from reactors and controls were placed in 2 mL crimp cap GC vials. Vials were inverted and temperature equilibrated at 25 °C. Headspace samples (100 μL) were removed manually using a sample-lock syringe (Hamilton) and analyzed with a HP 5890 GC equipped with GS-Q PLOT column (30 m, 0.545 mm, J&W Scientific) and FID. The injection split ratio was 10:1 and temperature was 230 °C. The oven temperature was 60 °C and the UHP He carrier gas flow rate was 5.5 mL/min. The detector temperature was 300 °C. Aqueous concentrations of ethane and ethene were calculated using dimensionless Henry's law constants at 25 °C as reported in literature (20.4 for ethane and 8.75 for ethene) [42]. The aqueous concentrations were further corrected for the fraction that partitioned into the 1 mL headspace of the reaction the reactor.

The same headspace method was used for analysis of hydrogen generated during the reactions for selected samples. Headspace samples (100 μL) equilibrated at 25 °C were manually injected into a HP 5890 GC equipped with a thermal conductivity detector, and a 10% SP1000 100/120 Carbosieve column (3.0 m, 3.2 mm, Supelco). The oven temperature was isothermal at 105 °C and the injector and detector temperatures were 200 °C. The aqueous concentration of hydrogen was calculated using the dimensionless Henry's law constant of 50.2 and aqueous concentrations were further corrected for the fraction that partitioned into the 1 mL headspace [43].

3. Results and discussion

3.1. H_2 evolution

To investigate hydrogen evolution during the oxidation of iron, water in the reactors was equilibrated with iron without adding the target compound and hydrogen formation was monitored. Fig. 1 shows the changes in the aqueous and total (aqueous + gas phase in 1 mL headspace) hydrogen concentration during the equilibration. With 0.02 g of iron added to 124 mL water, approximately 0.66 mM of hydrogen was accumulated in the reactor during the 22 h of equilibration, corresponding to 23% consumption of 2.89 mM (0.358 mmol) total iron available. Compared to a previous study [6], the iron investigated in this study produced approximately 30% more hydrogen per mass of iron during about 1 day of reaction. Presumably, this is due to the differences in chemical and physical characteristics of the particles that may stem from variability in particle preparation conditions. Assuming the observed hydrogen evolution rate is maintained (zero-order H_2 production), the projected lifetime of iron is only 96 h. However, it is apparent that the rate of hydrogen generation decreases toward the end of the equilibration time. This pattern of hydrogen evolution is consistent with that observed in previous studies and is attributed to changes in solution pH and surface passivation [6,7,9,44]. Iron metal corrosion typically

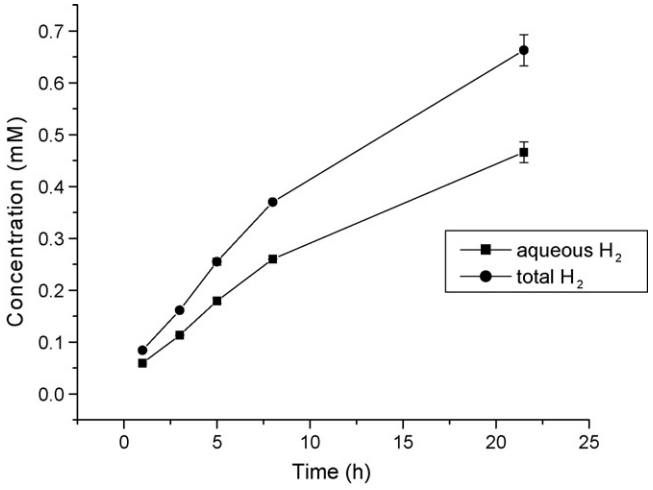

Fig. 1. Evolution of H_2 during the equilibration of 0.02 g nanoscale iron in 124 mL water. Symbols are the average concentrations from duplicate reactors or controls and error bars represent the range of concentrations. In some cases error bars are smaller than the symbol.

increases with decreasing pH and at higher pH surface precipitates contribute to passivation of the metal. Previous work has shown that the nanoscale iron investigated in this study shows increasing reactivity with chloroform and 1,1,2,2-tetrachloroethane with decreasing pH [11,45]. After 22 h reaction time, the solution pH had risen to 8.5, consistent with the observation of a lower hydrogen evolution rate. The development of a passivating layer would shift hydrogen evolution to a pseudo first-order process, resulting in an extended lifetime of iron. The reduced corrosion of nanoscale iron at high pH was also observed in a recent study which systematically investigated the effect of pH on hydrogen evolution and demonstrated pseudo-first-order behavior of hydrogen evolution [44]. Regarding the lifetime of nanoscale iron, Liu et al. [6] observed that nanoscale iron (≈97% Fe content), at the dose of 0.36 g Fe/L, continued to produce hydrogen up to 11 days of reaction. Also, Schrick et al. [9] predicted approximately 300 days lifetime of nanoscale nickel–iron (≈77% Fe content) at 3.3 g Fe/L, although their estimation was based on the measurements of hydrogen after the generation rate reached a plateau.

3.2. Reduction of chlorinated ethenes

Reduction experiments for chlorinated ethenes were carried out using 0.02 g of nanoscale iron in deionized water (non-equilibrated) and in water equilibrated with the iron for 24 h before target compound was added (equilibrated). Note that ‘‘equilibrated’’ does not mean the iron–water reaction reached equilibrium, but the iron was pre-exposed to water before the dechlorination was initiated. The transformation of chlorinated ethenes by nanoscale iron proceeded to fully dechlorinated ethene and ethane. Fig. 2 shows timecourses of TCE and *t*-DCE reduction in equilibrated water. It was assumed the reaction is not limited by mass transport of target compounds [46], and the experimental data for parent compound removal and products generation were simultaneously fit by nonlinear least squares methods using *Scientist for Windows* (v. 2.01, Micromath), assuming a parallel reduction pathway of the parent compound to ethene and ethane, while ethane is also produced from the reduction of ethene. TCE was primarily transformed to ethane, with no production of chlorinated byproducts. Ethene showed a typical behavior of reaction intermediate (initial increase followed by subsequent decrease). A similar pattern of reduction was observed for *t*-DCE reduction producing ethane as a major product and ethene as an intermediate. However, ethene was produced to higher concentrations than in the reduction of TCE. The branching ratios for the parallel reactions parent → ethene and parent → ethane (i.e., k_{ethene}/k_{ethane}), were 0.53(±0.12) and 0.83(±0.27) in the reduction of TCE and *t*-DCE, respectively. The dominance of saturated reaction products is similar to those observed for reactions involving catalytic reductants [22,47], and the increased ethene generation from lightly chlorinated ethenes is consistent with a Pd-catalyzed dechlorination [48].

The comparison of reaction rates of chlorinated ethenes in non-equilibrated and equilibrated water is shown in Fig. 3. The

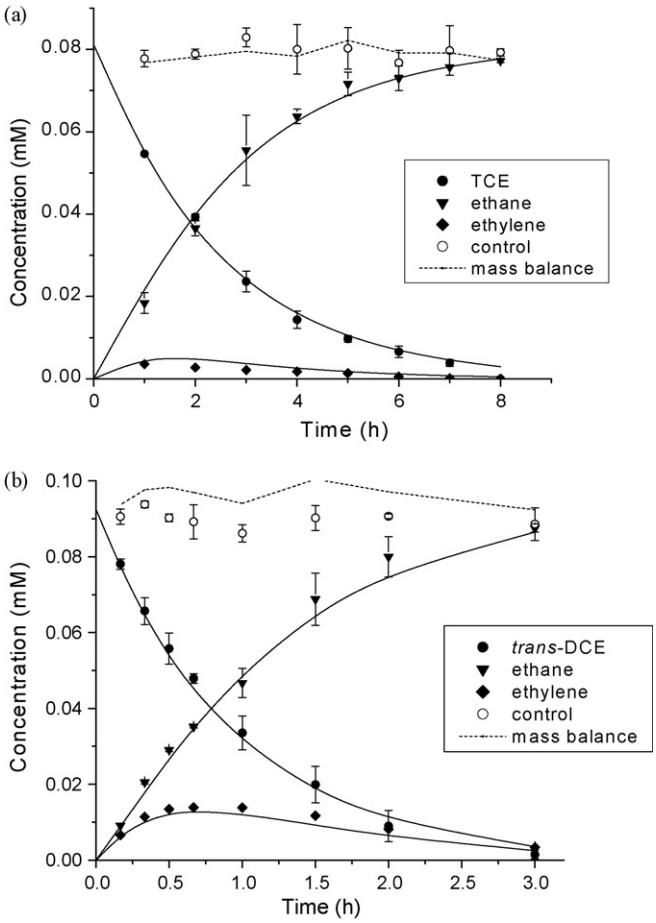

Fig. 2. Reduction of (a) TCE and (b) *t*-DCE by 0.02 g nanoscale iron in 124 mL equilibrated water. Smooth lines represent pseudo-first order fitting of data points. Symbols are the average concentrations from duplicate reactors or controls and error bars represent the range of concentrations. In some cases error bars are smaller than the symbol.

results indicate that, for a given compound, there is a substantial increase in the reaction rate in equilibrated water. The observed pseudo first-order rate constant (k_{obs}) values for all compounds increased by factors of 4–5, except PCE, for which the k_{obs}

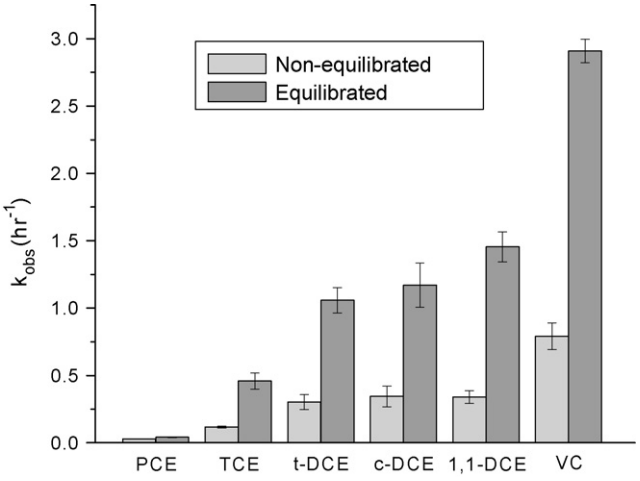

Fig. 3. Effect of equilibration on reduction of chlorinated ethenes by 0.02 g nanoscale iron in 124 mL water. Error bars represent 95% confidence limits.

increase was about a factor of 1.5. Such an increase in the reaction rate is likely due to the increased hydrogen concentration in the equilibrated reactors since the most notable change during the equilibration is buildup of hydrogen in the reactor (Fig. 1). Another possibility for increased reaction rate is that the iron itself underwent transformation process to form reactive surface moieties such as adsorbed Fe^{2+}, iron hydroxides, and green rust.

Along with the importance of equilibration, another interesting finding is that reaction rate increased with decreasing chlorination (VC > DCEs > TCE > PCE) in both equilibrated and non-equilibrated water. This is in contrast to the results of studies reported for micro-sized iron [49,50] although a few studies have reported increasing reaction rates with decreasing chlorination [36,46]. The reason for this disparity among previous studies regarding the effect of chlorination on relative reactivity is unclear. The trend of reactivity by nanoscale iron observed in this study is consistent with those observed for catalytic removal of chlorinated ethenes by bimetals (Pd–Fe, Ni–Fe) [24] and Pd catalyst [47,51]. The hydrodechlorination of chlorinated alkenes by catalysts has been proposed to be a two-step process that involves hydrogenation of the carbon double bond and the subsequent elimination of Cl, with the former being the rate-limiting step [48,52,53]. The faster kinetics of less chlorinated ethenes has been attributed to favored hydrogenation of the double bond through increased strength of the interaction between the π-orbital of the double bond and the d-orbital of the metal [51].

According to the proposed mechanism, however, the reduction of polychlorinated ethenes would produce partially chlorinated ethanes as reaction intermediates, which contrasts the product distribution obtained in this and other studies [47,48,54]. This would mean that, if the two-step process is the responsible mechanism, the chlorinated ethanes are anchored onto the surface until they become fully dechlorinated, or the reduction of those intermediates should be very rapid without releasing them to the solution. However, no evidence has been reported for such a strong interaction between chlorinated ethanes and catalytic surface. Further, the rate of dichloroethanes reaction with the same nanoscale iron used in this study was found to be extremely slow [45].

Regarding the absence of chlorinated ethanes formation, Ordonez et al. [53] suggested that removal of Cl coincides with H removal from the opposite carbon, and the double bond between the carbon atoms is re-established. However, their proposition is based on experiments performed in a solvent phase (*n*-heptane), and may not necessarily hold for reactions occurring in an aqueous phase since Cl by itself is a good leaving group in aqueous environments.

As an alternative to the two-step mechanism, Weiss and Krieger [55] investigated a gas phase dehydrochlorination of *c*- and *t*-DCE on a Pt catalyst and proposed a mechanism involving adsorption of substrates on the catalyst as tautomers (shift of the double bond to carbon–chlorine with the development of positive charge on chlorine and negative charge on carbon on the other side), hydrogenation of the carbon–chlorine double bond, and removal of HCl. They suggested DCEs are sequentially dechlorinated to ethene on the catalytic surface through the formation of the VC tautomer while the catalyst serves as a device for stabilizing the charge distribution of the tautomers. This mechanism may possibly explain the inverse correlation between reaction rate and chlorination of substrates, and absence of formation of chlorinated byproducts. However, similar to the two-step mechanism, the applicability of this mechanism to aqueous phase reaction is still in question since the formation of tautomers and the stabilizing effect of catalysts are likely to be reduced or prohibited by polarity of surrounding water molecules.

3.3. Effect of H_2

Fig. 4 presents the observed reaction rate constants of TCE reduction in reactors equilibrated for 0–12 h before the reaction was initiated by spiking TCE. The results indicate the reaction rate increased with increasing equilibration time. The observed rate constant appears to linearly increase up to 6 h equilibration but shows a sign of flattening out toward 12 h equilibration. This trend of reaction rate change is similar to the hydrogen concentration profile during the equilibration discussed earlier. The proportionality between reaction rate and equilibration time along with the good agreement of reaction rate with hydrogen concentration indicates hydrogen plays an important role in the reduction of by nanoscale iron. This behavior of TCE reduction and the importance of hydrogen are in agreement with previous studies [6,7].

The effect of hydrogen was investigated in a more systematic manner by reacting 0.07 mM TCE with 0.015 g nanoscale iron in 124 mL water with varying hydrogen concentration. A total of five combinations of conditions were set up to provide different hydrogen concentrations. These included (1) water purged with pure hydrogen then equilibrated with iron, (2) water equilibrated with iron, (3) water purged with hydrogen, (4) water not equilibrated with iron, and (5)

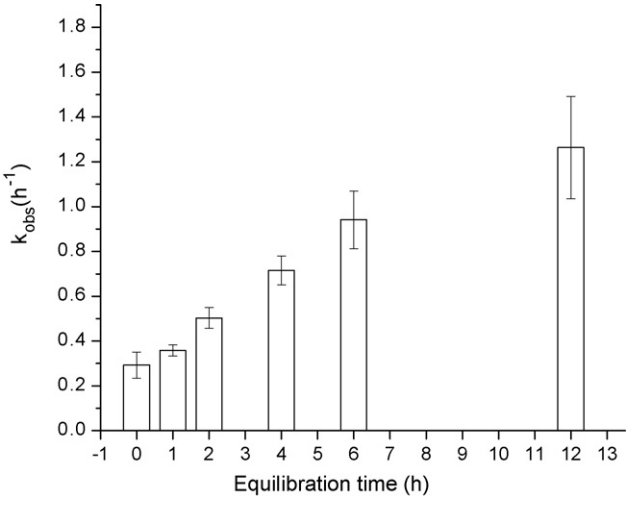

Fig. 4. Effect of equilibration time on reduction of 0.065 mM TCE by 0.05 g nanoscale iron. Error bars represent 95% confidence limits.

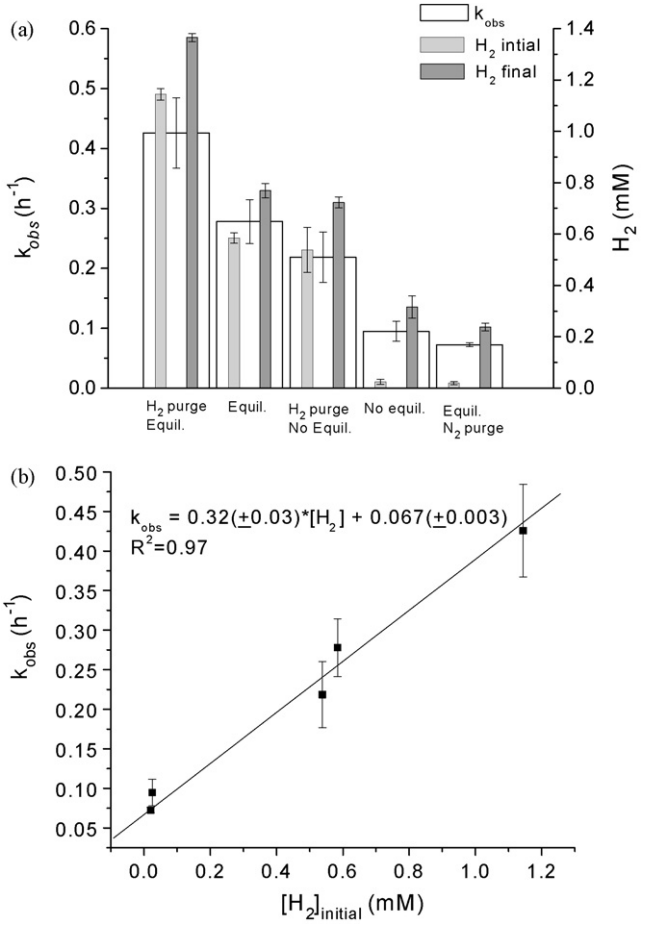

Fig. 5. (a) Effect of H_2 concentration on reduction of 0.07 mM TCE by 0.015 g nanoscale iron. (b) Correlation between initial hydrogen concentration and reaction rate constant. Error bars represent 95% confidence limits.

water equilibrated with iron followed by purging with nitrogen to remove hydrogen. The times for hydrogen purging, nitrogen purging, and equilibration with iron were approximately 3, 2, and 12–24 h, respectively. Reactor pH values just before addition of TCE were about 7.2 and 8.6 for non-equilibrated (3 and 4) and equilibrated (1, 2, and 5) conditions, respectively. Final pH values, after equilibration, if any, and approximately 8 h reaction time, ranged from 8.7 to 8.9 for the 10 reactors (two replicates each for five conditions).

Fig. 5 (a) shows pseudo-first order rate constants, and initial (at the beginning of reduction experiments) and final concentrations (after the reduction) of aqueous hydrogen in the reactors. For all five sets of conditions, initial hydrogen concentrations vary by a factor of approximately 60 and final concentrations by a factor of nearly 6, while for each condition, the increase in hydrogen during the reaction period is relatively constant (0.2 ± 0.04 mM). The correlation between reaction rate constant and initial hydrogen concentration is shown in Fig. 5(b). As the figure reveals, the reaction rate constants have a strong correlation with hydrogen concentration ($r^2 = 0.97$). A similar effect of hydrogen was observed for the reduction of *t*-DCE performed under the same experimental conditions (data not shown). Such a rate enhancing effect of hydrogen on TCE reduction was previously reported for a Pd catalyst [56] and Fe–B nanoparticles [6,7].

To investigate whether the catalytic pathway is operational in the reduction of haloalkanes, nanoscale iron was applied to 1,1,1,2-TeCA under varying hydrogen concentrations similar to TCE reduction. The pseudo-first-order reaction rate constants of 1,1,1,2-TeCA reduction at each condition are presented on Table 1, along with the rate constants of subsequent 1,1-DCE reduction, a major product of 1,1,1,2-TeCA reduction [45]. In contrast to TCE reduction, no definite trend in the rate constants of 1,1,1,2-TeCA reduction was found among the five conditions with different hydrogen concentrations, suggesting hydrogen was not directly involved in the reduction chlorinated ethanes. On the other hand, the subsequent reduction of 1,1-DCE shows significant dependence on the hydrogen concentration as observed in TCE reduction. In addition to chlorinated ethanes, the previous investigation with the same nanoscale iron showed that the reduction of chloroform was not affected by hydrogen concentration in the solution [11]. These observations suggest the reduction of haloalkanes does not proceed via catalytic hydrodechlorination, rather, it likely occurs via direct electron transfer from iron-associated surfaces to the physically adsorbed substrates, as suggested in previously reported studies [56,57].

The effect of hydrogen was further investigated with commercial grade micro-sized iron by reacting with TCE in water purged with/without hydrogen (conditions 3 and 4). The reduction was carried out at pH 8 using 50 mM MOPS buffer to rule out pH effect across the iron samples. The results presented in Fig. 6 show that for Connelly and Fisher irons, no effect of hydrogen on TCE reduction was observed. For ARS iron, hydrogen purging increased reaction rate by 8%, which may indicate a role of catalytic pathway; however, the increase is not statistically significant (it falls within the 95% confidence level), and is much smaller than that observed for nanoscale iron at similar hydrogen concentration increase. This suggests that, relative to nanoscale iron prepared using borohydride, the commonly used commercial irons utilize hydrogen very inefficiently, if at all, in catalytic reduction processes. Compared to amorphous nanoscale iron, the surface of commercial irons is likely to contain a number of crystalline surface oxides (e.g. Fe_2O_3, Fe_3O_4), lacking surface defects to

Table 1
Pseudo-first-order rate constants (h^{-1}) of reduction of 1,1,1,2-TeCA and 1,1-DCE (the reaction product of 1,1,1,2-TeCA reduction) by 0.01 g nanoscale iron under different reaction scenario

	H_2 purge + equilibrium	Equilibrium	H_2 purge + no equilibrium	No equilibrium	Equilibrium + N_2 purge
1,1,1,2-TeCA	1.23 (±0.08)	1.25 (±0.07)	1.17 (±0.09)	1.24 (±0.09)	1.10 (±0.07)
1,1-DCE	11.2 (±1.0) × 10^{-2}	5.1 (±0.7) × 10^{-2}	7.1 (±1.0) × 10^{-2}	3.6 (±0.6) × 10^{-2}	2.5 (±0.5) × 10^{-2}

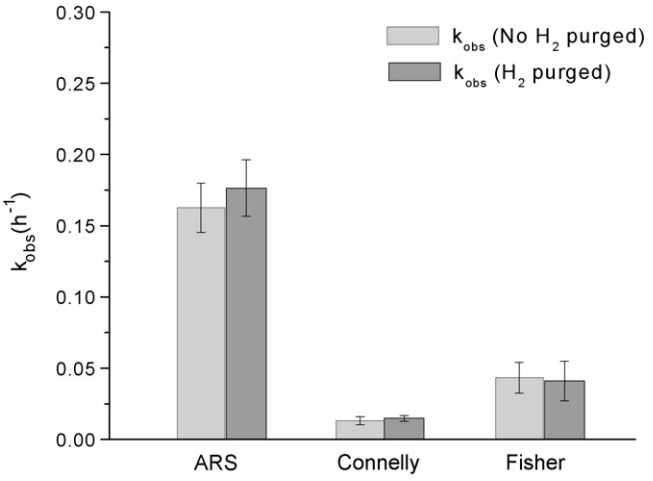

Fig. 6. Effect of hydrogen on reduction of 0.07 mM TCE by 5 g commercial grade iron pH 8. Error bars represent 95% confidence limits.

which hydrogen can adsorb [58], as well as lacking boron species that may impart catalytic capability. Liu et al. [6] observed a negligible effect of hydrogen with nanoscale iron particles composed of a crystalline insoluble Fe_3O_4 shell, which contrasted amorphous iron nanoparticles that showed a hydrogen utilizing capability. However, consideration of the catalytic-like result of increasing reaction rate with decreasing chlorination of ethenes (VC > DCEs > TCE > PCE) noted in a few studies using microscale electrolytic zero-valent iron [36,46], emphasizes the differences among these zero-valent irons and that a definitive study of a nanoscale iron equivalent in structure and composition to commonly used microscale irons has yet to be done.

4. Conclusions

Catalytic activity of laboratory synthesized nanoscale iron synthesized by borohydride reduction of ferric chloride was studied in the reduction of chlorinated ethenes. The evidence obtained in this study strongly suggests nanoscale iron transforms chlorinated ethenes via catalytic hydrodechlorination. The transformation of chlorinated ethenes by nanoscale iron proceeded to fully dechlorinated products (ethene and ethane), with no production of chlorinated intermediates. The reaction rates of chlorinated ethenes in water equilibrated with iron before the addition of substrates was 4–5 times greater than those in non-equilibrated water, except PCE which showed approximately 50% increase. The relative reaction rate of chlorinated ethenes (VC > DCEs > TCE > PCE) provides additional evidence of a catalytic pathway in that the rate of reaction was inversely proportional to the number of chlorine atoms to be removed from the molecules. The result of TCE reduction performed under five different hydrogen concentrations showed the reaction rate to be proportional to the initial hydrogen concentration in the reactor. In contrast to chlorinated ethenes, reduction of chlorinated ethanes was not influenced by hydrogen concentration, suggesting the reduction of haloalkenes by nanoscale iron does not proceed via catalytic hydrodechlorination, rather, it likely occurs via direct electron transfer reaction. TCE reduction by commercial grade microsized iron samples showed limited sensitivity to hydrogen concentration, suggesting the nanoscale iron synthesized by borohydride reduction is particularly reactive through a catalytic pathway involving hydrogen.

Acknowledgements

This work was supported by the National Science Foundation (award 996394) and the South Carolina Commission on Higher Education (award R00-C05). The authors gratefully acknowledge gifts of iron metal samples from ARS Technologies, Inc. and Connelly GPM, Inc. The authors also thank Drs. Tanju Karanfil and Sayed Dastgheib for their technical support in iron particle analysis.

References

[1] N.E. Korte, J.L. Zutman, R.M. Schlosser, L. Liang, B. Gu, Q. Fernando, Waste Manage. 20 (2000) 687–694.
[2] C.J. Lin, S.L. Lo, Y.H. Liou, J. Hazard. Mater. 116 (2004) 219–228.
[3] R. Muftikian, K. Nebesny, Q. Fernando, N. Korte, Environ. Sci. Technol. 30 (1996) 3593–3596.
[4] Y.H. Kim, E.R. Carraway, Environ. Technol. 24 (2003) 69–75.
[5] C.B. Wang, W.X. Zhang, Environ. Sci. Technol. 31 (1997) 2154–2156.
[6] Y. Liu, S.A. Majetich, R.D. Tilton, D.S. Sholl, G.V. Lowry, Environ. Sci. Technol. 39 (2005) 1338–1345.
[7] Y. Liu, H. Choi, D. Dionysiou, G.V. Lowry, Chem. Mater. 17 (2005) 5315–5322.
[8] J.T. Nurmi, P.G. Tratnyek, V. Sarathy, D.R. Baer, J.E. Amonette, K. Pecher, C.M. Wang, J.C. Linehan, D.W. Matson, R.L. Penn, M.D. Driessen, Environ. Sci. Technol. 39 (2005) 1221–1230.
[9] B. Schrick, J.L. Blough, A.D. Jones, T.E. Mallouk, Chem. Mater. 14 (2002) 5140–5147.
[10] G.V. Lowry, K.M. Johnson, Environ. Sci. Technol. 38 (2004) 5208–5216.
[11] H. Song, E.R. Carraway, Environ. Eng. Sci. 23 (2006) 272–284.
[12] D.W. Elliott, W.X. Zhang, Environ. Sci. Technol. 35 (2001) 4922–4926.
[13] C.L. Geiger, C.A. Clausen, K. Brooks, C. Klausen, C. Huntley, L.B. Filipek, D.D. Reinhart, J. Quinn, T. Krug, S. O'Hara, D. Major, Chlorinated Solvent and DNAPL Remediation: Innovative Strategies for Subsurface Cleanups, in: S.M. Henry, S.D. Warner (Eds.), ACS Symposium Series, American Chemical Society, Washington DC, (2003), pp. 939–944.
[14] K.W. Henn, D.W. Waddill, Remediation 16 (2006) 57–77.
[15] A.R. Gavaskar, L. Tatar, W. Condit, Cost and Performance Report: Nanoscale Zero-Valent Iron Technologies for Source Remediation (CR-05-007-ENV), Naval Facilities Engineering Command, Port Hueneme, CA, 2005.
[16] N. Saleh, K. Sirk, Y. Liu, T. Phenrat, B. Dufour, K. Matyjazewski, R.D. Tilton, G.V. Lowry, Environ. Eng. Sci. 24 (2007) 45–57.
[17] K.J. Klabunde, J. Stark, O. Koper, C. Mohs, D.G. Park, S. Decker, Y. Jiang, I. Lagadic, D.J. Zhang, J. Phys. Chem. 100 (1996) 12142–12153.
[18] H.L. Lien, W.X. Zhang, Colloids Surf., A 191 (2001) 97–105.
[19] H.L. Lien, W.X. Zhang, J. Environ. Eng. 131 (2005) 4–10.
[20] R. Muftikian, Q. Fernando, N. Korte, Water Res. 29 (1995) 2434–2439.
[21] C.H. Wan, Y.H. Chen, R. Wei, Environ. Toxicol. Chem. 18 (1999) 1091–1096.
[22] A.C. Grenier, M.M. McGuire, D.H. Fairbrother, A.L. Roberts, Environ. Eng. Sci. 21 (2004) 421–435.
[23] Y.H. Kim, E.R. Carraway, Environ. Technol. 24 (2003) 809–819.
[24] J.P. Fennelly, A.L. Roberts, Environ. Sci. Technol. 32 (1998) 1980–1988.
[25] S.J. Bransfield, D.M. Cwiertny, A.L. Roberts, D.H. Fairbrother, Environ. Sci. Technol. 40 (2006) 1485–1490.

[26] Y.H. Liu, F.L. Yang, J.W. Chen, L.N. Gao, G.H. Chen, Chemosphere 50 (2003) 1275–1279.
[27] X.H. Xu, H.Y. Zhou, P. He, D.H. Wang, Chemosphere 58 (2005) 1135–1140.
[28] J. Morales, R. Hutcheson, I.F. Cheng, J. Hazard. Mater. 90 (2002) 97–108.
[29] Y.H. Kim, E.R. Carraway, Environ. Sci. Technol. 34 (2000) 2014–2017.
[30] Y.H. Kim, W.S. Shin, S.O. Ko, J. Environ. Sci. Health, A 39 (2004) 1177–1188.
[31] I.F. Cheng, Q. Fernando, N. Korte, Environ. Sci. Technol. 31 (1997) 1074–1078.
[32] G.V. Lowry, M. Reinhard, Environ. Sci. Technol. 35 (2001) 696–702.
[33] T.P. Perng, J.K. Wu, Mater. Lett. 57 (2003) 3437–3438.
[34] J.K. Wu, Int. J. Hydrogen Energy 17 (1992) 917–921.
[35] T. Li, J. Farrell, Environ. Sci. Technol. 35 (2001) 3560–3565.
[36] J. Farrell, N. Melitas, M. Kason, T. Li, Environ. Sci. Technol. 34 (2000) 2549–2556.
[37] L. Gui, R.W. Gillham, M.S. Odziemkowski, Environ. Sci. Technol. 34 (2000) 3489–3494.
[38] H.X. Li, H. Li, W.L. Dai, M.H. Qiao, Appl. Catal., A 238 (2003) 119–130.
[39] Y.D. Wang, X.P. Ai, Y.L. Cao, H.X. Yang, Electrochem. Commun. 6 (2004) 780–784.
[40] G.N. Glavee, K.J. Klabunde, C.M. Sorensen, G.C. Hadjipanayis, Inorg. Chem. 34 (1995) 28–35.
[41] S.M. Ponder, J.G. Darab, J. Bucher, D. Caulder, I. Craig, L. Davis, N. Edelstein, W. Lukens, H. Nitsche, L.F. Rao, D.K. Shuh, T.E. Mallouk, Chem. Mater. 13 (2001) 479–486.
[42] D. Mackay, W.Y. Shiu, J. Phys. Chem. Ref. Data 10 (1981) 1175–1199.
[43] D.R. Lide, H.P.R. Frederikse, CRC Handbook of Chemistry and Physics, CRC Press Inc., Boca Laton, FL, 1995.
[44] Y. Liu, G.V. Lowry, Environ. Sci. Technol. 40 (2006) 6085–6090.
[45] H. Song, E.R. Carraway, Environ. Sci. Technol. 39 (2005) 6237–6245.
[46] W.A. Arnold, A.L. Roberts, Environ. Sci. Technol. 34 (2000) 1794–1805.
[47] G.V. Lowry, M. Reinhard, Environ. Sci. Technol. 33 (1999) 1905–1910.
[48] C.G. Schreier, M. Reinhard, Chemosphere 31 (1995) 3475–3487.
[49] R.W. Gillham, S.F. O'Hannesin, Ground Water 32 (1994) 958–967.
[50] T.L. Johnson, M.M. Scherer, P.G. Tratnyek, Environ. Sci. Technol. 30 (1996) 2634–2640.
[51] S. Ordonez, F.V. Diez, H. Sastre, Ind. Eng. Chem. Res. 41 (2002) 505–511.
[52] A.R. Pinder, Synthesis-Stuttgart 79 (1980) 425.
[53] S. Ordonez, H. Sastre, F.V. Diez, Appl. Catal., B 25 (2000) 49–58.
[54] E. Lopez, S. Ordonez, F.V. Diez, Appl. Catal., B 62 (2006) 57–65.
[55] A.H. Weiss, K.A. Krieger, J. Catal. 6 (1966) 167–185.
[56] T. Li, J. Farrell, Environ. Sci. Technol. 34 (2000) 173–179.
[57] L.J. Matheson, P.G. Tratnyek, Environ. Sci. Technol. 28 (1994) 2045–2053.
[58] A.J. Davenport, L.J.O. Oblonsky, H.P. Ryan, M.F. Toney, J. Electrochem. Soc. 147 (2000) 2162–2173.